From Heterogeneous to Homogeneous Nucleation of Isotactic Poly(propylene) Confined to Nanoporous Alumina

ARTICLE *in* NANO LETTERS · FEBRUARY 2011

Impact Factor: 13.59 · DOI: 10.1021/nl200153c · Source: PubMed

NANO LETTERS

LETTER

pubs.acs.org/NanoLett

From Heterogeneous to Homogeneous Nucleation of Isotactic Poly(propylene) Confined to Nanoporous Alumina

Hatice Duran,[†,‡] Martin Steinhart,[§] Hans-Jürgen Butt,[†] and George Floudas*[,∥,⊥]

[†]Max Planck Institute for Polymer Research, Ackermannweg 10, 55128 Mainz, Germany

[‡]TOBB University of Economics and Technology, Ankara, Turkey

[§]Institut fuer Chemie, Universitaet Osnabrueck, D-49069 Osnabrueck, Germany

[∥]Department of Physics, University of Ioannina, 451 10 Ioannina, Greece

[⊥]Foundation for Research and Technology (FORTH), Biomedical Research Institute, Ioannina, Greece

Supporting Information

ABSTRACT: The crystallization of highly isotactic polypropylene confined in self-ordered nanoporous alumina is studied by differential scanning calorimetry. A transformation from a predominantly heterogeneous to predominantly homogeneous nucleation takes place if the pore diameter is smaller than 65 nm. Crystallization is suppressed with decreasing pore size, and the absence of nucleation below 20 nm pores indicates the critical nucleus size. The results reported here might enhance the understanding of nanocomposites containing semicrystalline polymers and reveal design criteria for polymeric nanofibers with tailored mechanical and optical properties.

KEYWORDS: Nucleation, constrained crystallization, nanoporous alumina, isotactic polypropylene, calorimetry

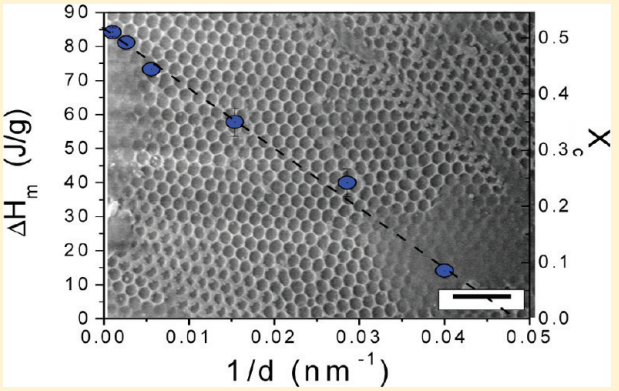

It is known that a size limitation in the nanometer scale can affect the energetics involved in crystal nucleation, growth, and orientation.[1,2] As an example we mention the controlled crystal orientation in semicrystalline polymers.[3−9] Polymer crystallization under confinement can be substantially different from the bulk and to the extent that the final mechanical and optical material properties are influenced by the degree of crystallinity this can have important technological applications. Bulk crystallization proceeds usually via heterogeneous nucleation and gives rise to structure over multiple length scales: from the crystalline unit cell (1−2 nm), to alternating crystalline/amorphous lamellae (50−100 nm)[10−12] and to spherulitic superstructures (>500 nm and up to centimeters).[13,14] In *heterogeneous* nucleation the process initiates at defects or impurities extrinsic to the pure material. This is the dominant nucleation mechanism in bulk polymers. *Homogeneous* nucleation, on the other hand, is more rare but intrinsic to the polymer and requires larger supercooling so that the driving force for crystallization overcomes the intrinsic barrier to nucleation.

The motivation for this work has been studies of polymer crystallization confined to droplets[6,15,16] and within the spherical nanodomains of block copolymers[17,5,6] by X-ray scattering,[17] differential scanning calorimetry (DSC),[6] polarizing optical microscopy (POM),[15,16] and atomic force microscopy (AFM).[5] These studies emphasized the interplay between heterogeneous and homogeneous nucleation and explored the kinetics of homogeneous nucleation observed at high supercooling. The droplet experiments in particular, apart from providing a neat way of separating homogeneous from hererogeneous nucleation, have also shown that the probability of nucleation depends on the volume of droplets and not on their surface area.[15,16]

Nanoporous aluminum oxide (AAO)[18−20] has been widely used as an inorganic model matrix as it contains arrays of straight cylindrical nanopores, uniform in length and diameter, that can easily be infiltrated with polymeric melts.[21] It is already known that segmental dynamics of polymers is altered in the presence of the hard pore walls of AAO.[22,23] With respect to polymer crystallization, some authors have reported heterogeneous surface nucleation of polyethylene confined to AAO nanopores small enough to neglect the presence of other types of heterogeneous nuclei.[24,25] This finding leads to several questions about the type of nucleation under hard confinement typical for AAO: Is the crystallization process always heterogeneous within the small AAO nanopores? Can hard confinement completely suppress polymer crystallization and if so what is the required size? In this Letter we explore these issues using highly isotactic polypropylene (iPP) confined within the nanopores of self-ordered AAO having dimensions ranging from 380 to 25 nm. Strikingly, we show that crystallization of iPP is expected to be completely suppressed inside pores with diameters of 20 nm and below.

Received: January 14, 2011
Revised: February 18, 2011
Published: February 28, 2011

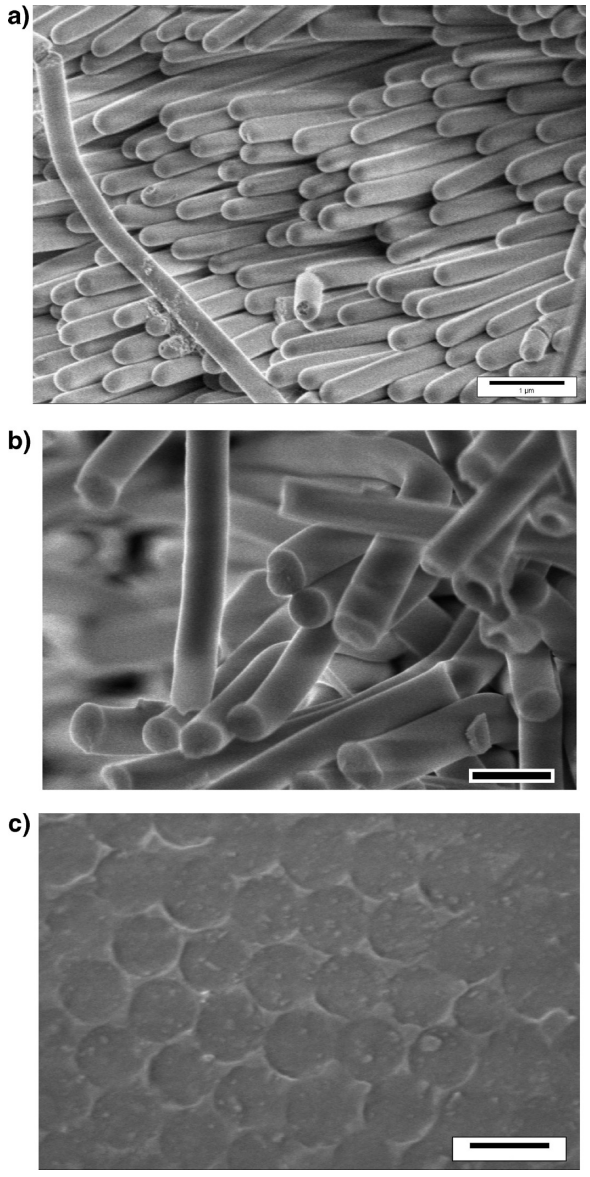

Figure 1. Scanning electron microscopy images of iPP nanorods prepared in self-ordered AAO with a pore depth of 80 nm and a pore diameter of 380 nm. (a) Tips of released iPP nanorods, which are replicas of the pore bottoms of the self-ordered AAO. The self-ordered AAO was etched with aqueous KOH solution. (b) Fractured iPP nanorods; (c) surface of infiltrated self-ordered AAO containing iPP nanorods after removal of excess polymer. The dark scale bars are 500 nm.

The iPP (Polymer Standards Service, Mainz, product code: PSS-ppb105k) had a mass-average molecular weight M_w = 108000 g/mol, a number-average molecular weight M_n = 32500 g/mol, a molar mass at the SEC peak maximum M_p = 82800 g/mol, and a polydispersity index M_w/M_n = 3.32. The high isotactic *mmmm* content of the iPP of ~99% was verified by ^{13}C NMR spectroscopy on *o*-$C_6D_4Cl_2$ solutions at 393 K (Supporting Information, Figure S1). The real-time crystallization and melting of the bulk iPP was followed by polarizing optical microscopy (POM).[26] The analysis of the crystallization kinetics resulted in an estimate for the equilibrium melting temperature (Supporting Information Figures S2 and S3) as T_m^0 = 461 K.[26] Wide-angle X-ray scattering patterns of bulk iPP showed (110), (040), (130), ($\bar{1}$31)/(111), and (060) reflections corresponding to the monoclinic α-iPP (unit cell parameters of a = 0.665 nm, b = 2.076 nm, c = 0.65 nm, with β = 98.67°, α = γ = 90°).[27] A weak peak corresponding to the (117) reflection of the γ form (triclinic) of iPP was also observed as a minor feature.

Self-ordered AAO (pore diameters of 25, 35, 65, 180, and 380 nm; pore depth 80−100 μm) was prepared following the procedures reported in the literature.[18−20,28] Infiltration of the iPP was performed by placing neat iPP on the surface of the self-ordered AAO at 473 K for 20 h under vacuum or argon atmosphere. Scanning electron microscopy (SEM) investigations using a LEO Gemini 1530 SEM, operated at acceleration voltages from 0.75 to 6 kV, revealed that under the conditions applied the pores of the self-ordered AAO were filled with iPP down to the bottom. For example, the convex hemispherical tips of the iPP nanorods released from self-ordered AAO with pore diameter of 380 nm and a pore depth of 80 μm, seen in Figure 1a, are a replica of the concave pore bottoms of the self-ordered AAO. Fractured iPP nanorods unveiled their solid nature, as seen in Figure 1b. Prior to the crystallization kinetics experiments, excess iPP was removed from the surface of the self-ordered AAO membranes with sharp razor blades and soft polishing paper (Buehler Microcloth). As a result, the mouths of the self-ordered AAO pores containing solid iPP nanorods were uncovered (Figure 1c). Hence, during the DSC experiments separated iPP entities were located inside the pores of the self-ordered AAO.

Thermal analysis was carried out using a Mettler Toledo differential scanning calorimeter (DSC-822). A 3−10 mg portion of sample material was sealed in aluminum pans (100 μL). DSC traces of neat iPP were acquired using an empty aluminum pan as reference. The iPP mass in iPP-infiltrated AAO was estimated from the mass difference between iPP-infiltrated self-ordered AAO and empty self-ordered AAO pieces having the same size and the same pore diameter. DSC traces of iPP-infiltrated self-ordered AAO were recorded using reference pans containing empty AAO pieces having the same size and pore diameter. All samples were first cooled at a rate of 10 K/min from ambient temperature to 223 K and then heated to 503 K at the same rate under a nitrogen atmosphere. The same cycle was repeated two times. Melting and crystallization points, as well as heats of fusion and of crystallization were determined from the second heating and cooling thermographs. In isothermal crystallization experiments, the crystalline mass fraction, $W(t)$, was estimated as

$$W(t) = \frac{\int_0^t \left(\frac{dH_c}{dt}\right) dt}{\int_0^\infty \left(\frac{dH_c}{dt}\right) dt} \quad (1)$$

where the numerator is the heat generated at time t and the denominator is the total heat generated at the end of the isothermal crystallization at the respective temperature. The crystalline mass fraction thus obtained is related to the volumetric fraction, V_c, as[29]

$$V_c = \frac{W(t)}{\left[W(t) + \left(\frac{\rho_c}{\rho_a}\right)(1 - W(t))\right]} \quad (2)$$

where ρ_c and ρ_a are the density of fully crystalline (0.946 g/cm^3) and fully amorphous (0.853 g/cm^3) polypropylene, respectively.[30]

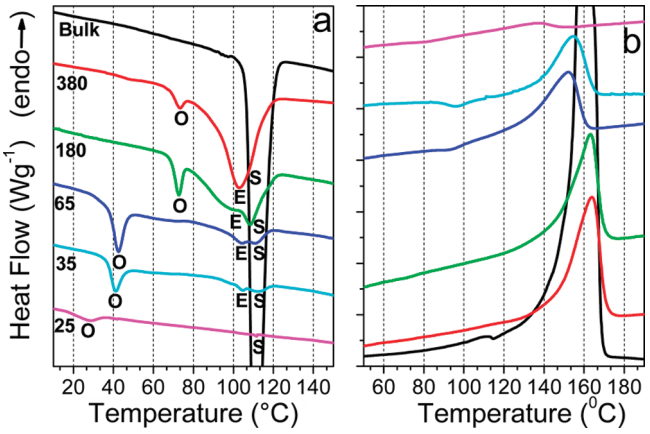

Figure 2. Cooling (a) and subsequent heating (b) thermograms of bulk iPP and of iPP located inside self-ordered AAO with pore diameters ranging from 380 to 25 nm (heating and cooling rate, 10 K/min). The letters S, E, and O denote peaks originating from excess material on the AAO surface, crystallization initiated by heterogeneous nucleation and crystallization initiated by homogeneous nucleation, respectively.

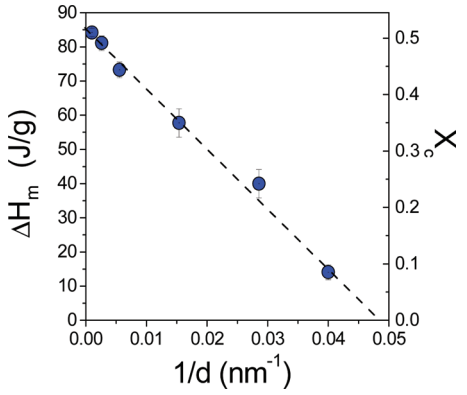

Figure 3. (Left) Heat of fusion of iPP plotted as a function of inverse self-ordered AAO pore diameter. Vertical right axis: degree of crystallinity as a function of inverse AAO pore diameter (calculations are based on the heat of fusion of 100% crystalline iPP, which amounts to 165 J/g).

In the isothermal crystallization experiments all samples were first heated to 473 K and held at this temperature for 10 min to eliminate any previous thermal history, followed by rapid cooling to the final crystallization temperature (T_c) with a rate of 100 K/min. The samples were kept at the crystallization temperature for 45 min and then heated again to 473 K with a rate of 2 K/min.

Figure 2 shows cooling and subsequent heating traces taken at a rate of 10 K/min. On cooling, bulk iPP shows a strong exothermic crystallization peak at 108.8 °C. In self-ordered AAO with a pore diameter of 380 nm the exothermic peak is broadened and shifted to 103.1 °C. In addition, a second—albeit weak—exothermic process appears at 73.1 °C. The trace for iPP-infiltrated self-ordered AAO with a pore diameter of 180 nm is similar, apart from the occurrence of two exothermic peaks at higher temperatures (at 108.5 and 99 °C). The traces of iPP infiltrated into self-ordered AAO with pore diameters of 65, 35, and 25 nm are distinctly different. The high temperature exothermic peak is very weak, whereas the low-temperature exothermic peak shifts to even lower temperatures, broadens, and loses intensity upon confinement. In the case of iPP residing inside self-ordered AAO with a pore diameter of 25 nm, the low temperature peak, being the main feature in the DSC trace, is shifted to 28.9 °C.

The origin of the high- and low-exothermic peaks can be understood if we consider the relation between the volume of a pore and the volume per nucleus in bulk iPP. A typical spherulitic diameter for iPP (crystallized at 70 °C)[31] is in the order of 10 μm giving a volume per nucleus of about 5×10^{-7} mm^3. With this density of defects bulk iPP crystallizes solely via heterogeneous nucleation. The iPP-infiltrated self-ordered AAO with 380 nm pores crystallizes mainly by *heterogeneous* nucleation since the pore volume ($\sim 10^{-8}$ mm^3) is close to the volume per nucleus in the bulk sample. However, not all pores contain impurities; thus *homogeneous* nucleation appears at lower temperatures for iPP chains in those pores that are free from defects. In the other extreme, self-ordered AAO with pores 25 nm in diameter, the pore volume ($\sim 5 \times 10^{-11}$ mm^3) is much smaller than the volume per nucleus in bulk iPP; thus it will crystallize mainly by homogeneous nucleation as experimentally observed. It seems that the transition from predominantly heterogeneous to predominantly homogeneous nucleation occurs at pore diameters of about 65 nm with a pore volume corresponding to 1‰ of the volume per heterogeneous nucleus in bulk iPP. Hence in Figure 2a, O and E denote homogeneous and heterogeneous nucleation, respectively. The exothermic peak at 108.8 °C, appearing even in the case of iPP-infiltrated self-ordered AAO with a pore diameter of 25 nm, can be ascribed to a small amount of iPP on the surface (S) of the self-ordered AAO membranes that melts at the same temperature as bulk iPP. This small amount of iPP cannot induce crystallization in the pores as lamellae originating from nuclei outside the AAO pores need to hit the pores at a certain orientation.[8] Furthermore, the low temperature peak did not shift in several consecutive cooling runs, reflecting intrinsic (i.e., homogeneous) nucleation. It should be mentioned here that these effects are reminiscent to the interplay between homogeneous and heterogeneous nucleation observed in poly(ethylene oxide) confined to droplets.[15,16]

On subsequent heating (Figure 2b), the thus crystallized bulk iPP melts with a double endothermic peak possibly indicating the occurrence of different crystal thicknesses and/or of melting/recrystallization processes. In the case of iPP confined to self-ordered AAO, the endothermic peak is very broad and asymmetric toward the low temperature side, reflecting the melting of homogeneously and heterogeneously formed crystals, as well as the possible reorganization/perfection of crystals, as previously revealed by AFM,[5] DSC,[6] and POM[15,16] studies on confined crystallization in block copolymers and droplets, respectively. The heat of fusion (averages over several runs) strongly decreases as the pore diameter decreases (Figure 3). Linear extrapolation reveals that iPP-infiltrated into self-ordered AAO with pore diameters below about 20 nm would be unable to nucleate. This diameter can be employed as an estimate of the dimension of the critical nucleus that corresponds to about 10 unit cells (see below). Alternatively, the longitudinal dimension of the critical nucleus, l^*, can be obtained from[29] $l^* = 4\sigma_e T_m^0 / \Delta T \Delta H_m \rho_c$, where, σ_e (=0.146 J/m^2) is the fold surface free energy, T_m^0 (=461 K) is the equilibrium melting temperature, ΔH_m (=165 J/g) is the latent heat of fusion at the equilibrium melting temperature, $\Delta T = (T_m^0 - T_c)$ is the undercooling and ρ_c (=0.946 g/cm^3) the crystal density. Thus, a critical nucleus size of 10−12 nm is obtained for homogeneous nucleation in nanopores, which is in reasonable agreement with the above estimate. Interestingly, the smaller nodular crystals in isotactic

dx.doi.org/10.1021/nl200153c |*Nano Lett.* 2011, 11, 1671–1675

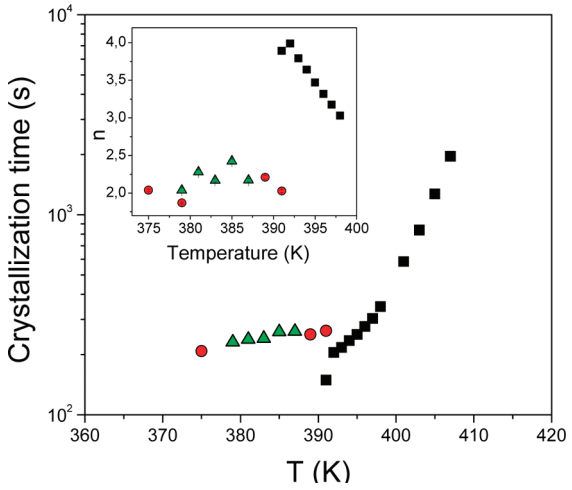

Figure 4. Crystallization times obtained from the isothermal crystallization experiments: bulk iPP, squares; iPP inside self-ordered AAO with a pore diameter of 380 nm, circles; and iPP inside self-ordered AAO with a pore diameter of 180 nm, up triangles. The inset displays the Avrami exponent n as a function of temperature.

polypropylene observed by AFM[32] had a size of ~20 nm, i.e., comparable to the critical nucleus size. The here predicted complete suppression of crystallization within the one-dimensional hard confinement of self-ordered AAO, contrasts with results reported for two-dimensional crystallization of poly(ethylene oxide)[4] and polypropylene[33] in multilayer nanoassemblies. These experiments revealed that the polymers could still crystallize as single lamellae with large aspect ratios. In addition, PEO nucleation was uninhibited down to ~10 nm confinement in all three dimensions.[34] Dimensionality of confinement and intrinsic polymer mobility are issues that need to be explored further.

The presence of a strong exothermic peak due to heterogeneous nucleation in bulk iPP and iPP confined to self-ordered AAO with diameters of 380 and 180 nm allows comparing the (heterogeneous) crystallization kinetics in bulk and under confinement. The analysis of the isothermal crystallization kinetics is performed with the classical Avrami equation:[35]

$$V_c(t) = 1 - \exp(-kt^n) \qquad (3)$$

The volumetric fraction was determined according to eq 2. In eq 3, k and n reflect the crystallization rate constant and the Avrami exponent, respectively. The crystallization rate constant, k, yields the half-time of crystallization as $t_{1/2} = (\ln 2/k)^{1/n}$. The Avrami exponent, n, is considered to represent the dimensionality of the growing crystals (a value of 3 corresponds to unrestricted three-dimensional crystal growth, a value of 1 to one-dimensional crystal growth, e.g., along a capillary) as well as the time dependence of nucleation (0 corresponds to instantaneous, athermal nucleation and 1 to purely sporadic, thermal nucleation). The crystallization process in bulk iPP could be very well described with eq 3 up to 50% conversion associated with primary crystallization,[36] and the kinetic times and Avrami exponents are plotted in Figure 4. The Avrami exponent of bulk iPP varies from 4 to about 3 as the crystallization temperature increases from 390 to 398 K. The noninteger values reflect spherulitic growth from a mixture of "instantaneous" with "sporadic" nuclei. Nucleation in self-ordered AAO with pore diameters of 380 and 180 nm was analyzed using eq 3, and the results were compared with the situation in bulk iPP (cf. Figure 4). Crystallization kinetics under confinement is characterized by two main effects: slower characteristic times and reduced values of n. The latter reflect the restricted crystal growth by the cylindrical shape of the nanopores. We note here that a much stronger effect was found for the *homogeneous* crystallization within droplets,[15] in rigid nanochannels,[8] and within the spherical nanodomains of block copolymers[17] (with Avrami exponent $n = 1$). Here, the small heat of fusion and the higher supercooling needed[37,38] for the homogeneous nucleation precluded a similar investigation of the low temperature peak.

In summary, crystallization in separated nanorods consisting of highly isotactic polypropylene inside nanoporous alumina is predominantly initiated by heterogeneous nucleation if the pore diameters are larger than 65 nm. Inside pores having diameters below 65 nm, predominantly homogeneous nucleation initiates crystallization. Nucleation is completely suppressed in pores having diameters below about 20 nm since under such strong confinement the surface energy of the crystals would prevail over their inherent energy. This outcome is of technological relevance for the understanding of nanocomposites containing semicrystalline polymers as well as for the design of polymeric nanofibers with tunable mechanical strength, processability, and optical clarity.

■ ASSOCIATED CONTENT

Supporting Information. Experimental details on (i) the polymer tacticity and (ii) the equilibrium melting point and bulk iPP crystallization kinetics. This material is available free of charge via the Internet at http://pubs.acs.org.

■ AUTHOR INFORMATION

Corresponding Author
*E-mail: gfloudas@cc.uoi.gr.

■ ACKNOWLEDGMENT

Technical support by Dr. M. Mondeshki (NMR), K. Sklarek (self-ordered AAO membranes), G. Glasser (SEM), and J. Thiel (DSC) are gratefully acknowledged. G.F. acknowledges financial support by the John S. Latsis public benefit Foundation. H.D. and M.S. gratefully acknowledge financial support from the German Research Foundation (SPP 1369).

■ REFERENCES

(1) Turnbull, D. *J. Chem. Phys.* **1950**, *18*, 198–203.
(2) Schmelzer, J. W. P.; Abyzov, A. S. *J. Chem. Phys.* **2011**, *134*, No. 054511.
(3) Hu, Z.; Baralia, G.; Bayot, V.; Gohy, J.-F.; Jonas, A. M. *Nano Lett.* **2005**, *5*, 1738–1743.
(4) Wang, H.; Keum, J. K.; Heltner, A.; Baer, E.; Freeman, B.; Rozanski, A.; Galeski, A. *Science* **2009**, *323*, 757–760.
(5) Reiter, G.; Castelein, G.; Sommer, J.-U.; Röttele, A.; Thurn-Albrecht, T. *Phys. Rev. Lett.* **2001**, *87*, No. 226101.
(6) Röttele, A.; Thurn-Albrecht, T.; Sommer, J.-U.; Reiter, G. *Macromolecules* **2003**, *36*, 1257–1260.
(7) Ma, Y.; Hu, W.; Hobbs, J.; Reiter, G. *Soft Matter* **2008**, *4*, 540–543.
(8) Steinhart, M.; Göring, P.; Dernaika, H.; Prabkukaran, M.; Gösele, U.; Hempel, E.; Thurn-Albrecht, T. *Phys. Rev. Lett.* **2006**, *97*, No. 027801.
(9) Wu, H.; Wang, W.; Huang, Y.; Su, Z. *Macromol. Rapid Commun.* **2009**, *30*, 194–198.

(10) Keller, A. *Philos. Mag.* **1957**, *2*, 1171.
(11) Strobl, G. *The Physics of Polymers*, 2nd ed.; Springer: Berlin, 1997.
(12) Cheng, S. Z. D.; Lotz, B. *Polymer* **2005**, *46*, 8662.
(13) Keith, H. D.; Padden, F. J. *J. Appl. Phys.* **1963**, *34*, 2409.
(14) Bassett, D. C.; Vaughan, A. S. *Polymer* **1985**, *26*, 717.
(15) Massa, M. V.; Dalnoki-Veress, K. *Phys. Rev. Lett.* **2004**, *92*, No. 255509.
(16) Massa, M. V.; Carvalho, J. L.; Dalnoki-Veress, K. *Eur. Phys. J. E: Soft Matter Biol. Phys.* **2003**, *12*, 111–117.
(17) Loo, Y.-L.; Register, R. A.; Ryan, A. J. *Phys. Rev. Lett.* **2000**, *84*, 4120–4123.
(18) Masuda, H.; Fukuda, K. *Science* **1995**, *268*, 1466–1468.
(19) Masuda, H.; Hasegawa, F.; Ono, S. *J. Electrochem. Soc.* **1997**, *144*, L127–L130.
(20) Masuda, H.; Yada, K.; Osaka, A. *Jpn. J. Appl. Phys.* **1998**, *37*, L1340–L1342.
(21) Steinhart, M. *Adv. Polym. Sci.* **2008**, *220*, 123.
(22) Duran, H.; Gitsas, A.; Floudas, G.; Mondeshki, M.; Steinhart, M.; Knoll, W. *Macromolecules* **2009**, *42*, 2881–2885.
(23) Martin, J.; Mijangos, C.; Sanz, A.; Ezquerra, T. A.; Nogales, A. *Macromolecules* **2009**, *42*, 5395–5401.
(24) Woo, E.; Huh, J.; Jeong, Y. G.; Shin, K. *Phys. Rev. Lett.* **2007**, *98*, No. 136103.
(25) Shin, K.; Woo, E.; Jeong, Y. G.; Kim, C.; Huh, J.; Kim, K.-W. *Macromolecules* **2007**, *40*, 6617–6623.
(26) Gitsas, A.; Floudas, G. *Macromolecules* **2008**, *41*, 9423–9429.
(27) Chen, J.-H.; Chang, Y.-L. *J. Appl. Polym. Sci.* **2007**, *103*, 1093–1104.
(28) Nielsch, K.; Choi, J.; Schwirn, K.; Wehrspohn, R. B.; Gösele, U. *Nano Lett.* **2002**, *2*, 677.
(29) Gedde, U. W. *Polymer Physics*; Chapman & Hall: London and New York, 1995.
(30) Wunderlich, B. *Macromolecular Physics*; Academic Press, Inc.: New York, 1973; Vol.1.
(31) Coccorullo, I.; Pantani, R.; Titomanlio, G. *Polymer* **2003**, *22*, 3007–318.
(32) Zia, Q.; Radusch, H. J.; Androsch, R. *Polymer* **2007**, *48*, 3504–3511.
(33) Jin, Y.; Rogunova, M.; Hiltner, A.; Baer, E.; Nowacki, R.; Galeski, A.; Piorkowska, E. *J. Polym. Sci., Polym. Phys. Ed.* **2004**, *42*, 3380–3396.
(34) Massa, M. V.; Carvalho, J. L.; Dalnoki-Veress, K. *Phys. Rev. Lett.* **2006**, *97*, No. 247802.
(35) >Avrami, M. >*J. Chem. Phys.* **1939**, *7*, 1103. Avrami, M. *J. Chem. Phys.* **1940**, *8*, 212. Avrami, M. *J. Chem. Phys.* **1941**, *9*, 177.
(36) Lorentzo, A. T.; Arnal, M. L.; Albuerne, J.; Müller, A. J. *Polym. Test.* **2007**, *26*, 222–231.
(37) Silvestre, C.; Cimmino, A.; Duraccio, D.; Schick, C. *Macromol. Rapid Commun.* **2007**, *28*, 875–881.
(38) De Santis, F.; Adamovsky, S.; Titomalio, G.; Schick, C. *Macromolecules* **2007**, *40*, 9026–9031.